High-precision temperature sensor using phase-shifted fiber Bragg grating written directly by femtosecond laser

LIJIE WANG,^{1,2} JUN HE,^{1,2} PRUNXIAO CHEN,^{1,2} HAO LUO,^{1,2} BAIJIE XU,^{1,2} XIZHEN XU,^{1,2} ZHIYONG BAI,^{1,2} AND YIPING WANG^{1,2,*}

 1 Key Laboratory of Optoelectronic Devices and Systems of Ministry of Education/Guangdong Province, College of Physics and Optoelectronic Engineering, Shenzhen University, Shenzhen 518060, China ²Shenzhen Key Laboratory of Photonic Devices and Sensing Systems for Internet of Things, Guangdong and Hong Kong Joint Research Centre for Optical Fibre Sensors, Shenzhen University, Shenzhen 518060, China *ypwang@szu.edu.cn

Abstract: A high-quality π -phase-shifted fiber Bragg grating (PSFBG) was inscribed in conventional single-mode fiber by use of femtosecond laser direct writing technology to demonstrate a high-precision temperature sensor. During grating inscription, the slit beam shaping technique was employed to reduce the 3 dB bandwidth of the grating's phase-shifted peak from 12.0 pm to 4.8 pm, thereby significantly enhancing the wavelength resolution of the fiber Bragg grating. Such a PSFBG exhibited a temperature sensitivity of 10.71 pm/°C, with an average standard deviation range of 0.005-0.016 °C for temperature measurements. This PSFBG represents a highly promising temperature sensor, featuring a minimum temperature resolution of 0.01 °C and a maximum temperature uncertainty of 0.016 °C. This outstanding performance is primarily attributed to the reduction of the PSFBG's birefringence from 5.607×10^{-5} to 2.247×10^{-6} using the slit beam shaping technique, which substantially enhances the stability of the resonant wavelength of the grating's phase-shifted peak and the measurement accuracy of the fiber Bragg grating temperature sensor.

© 2025 Optica Publishing Group under the terms of the Optica Open Access Publishing Agreement

Introduction

Environmental temperature is a critical parameter in real-time health monitoring of intelligent engineering structures, as subtle temperature changes can induce significant measurement errors in other parameters. In addition, high-precision temperature measurement and control are key factors in ensuring product quality and process stability in fields such as industrial manufacturing, electronics and semiconductors, biomedicine, environmental monitoring, and oil well exploration. Therefore, it is urgent to achieve high-resolution and high-precision temperature measurement. Conventional electrical temperature sensors offer relatively high precision but suffer from large size and vulnerability to electromagnetic interference, limiting their use in complex electromagnetic environments. Fiber optic sensors, characterized by small size, light weight, and electromagnetic interference immunity, have been widely adopted in precision measurement applications [1–4]. Among them, fiber Bragg gratings (FBGs) are typical fiber optic temperature sensors. However, conventional FBGs exhibit relatively large 3 dB bandwidths, leading to low wavelength resolution and thus limited temperature measurement precision. While increasing the grating length (number of periods) can narrow the 3 dB bandwidth, long FBGs may introduce chirp effects in practical use, degrading measurement accuracy [5].

Phase-shifted fiber Bragg gratings (PSFBGs), with their unique refractive index modulation profiles, feature ultra-narrow phase-shifted peaks in transmission spectra [6–11]. The 3 dB bandwidth of these peaks is typically one to two orders of magnitude smaller than the reflection

peaks of conventional FBGs with the same length, enabling temperature sensors with higher wavelength resolution and significantly improved temperature measurement precision [12–18]. For example, Chen [13] demonstrated high-resolution simultaneous measurement of temperature and strain using a π -phase-shifted FBG in a polarization-maintaining fiber, achieving a temperature resolution (standard deviation) of 0.0014 °C over a stable data segment. However, using the standard deviation of the most stable data segment as the sensor resolution is inappropriate for practical engineering applications. Sun [19] reported that the average temperature precision of an FBG and PSFBG integrated into an optical frequency domain reflectometry, is 0.13 and 0.05 °C, respectively. And the minimal temperature precision achieved by the PSFBG is 0.01 °C 0.105 pm, which is approximately one-eighth of the precision of FBG.

In this work, a π -phase-shifted FBG was written in a conventional single-mode fiber using femtosecond laser point-by-point technology. Slit beam shaping was employed to reduce the maximum polarization independence loss (PDL) from 25.6 to 2.9 dB and narrow the 3 dB bandwidth of the phase-shifted peak from 12.0 to 4.8 pm, significantly enhancing the wavelength resolution in temperature measurement. Moreover, a polarization analysis system with picometer-level wavelength resolution and a thermostatic water bath were used to accurately characterize the temperature response of the PSFBG, achieving a temperature sensitivity of 10.71 pm/°C. High-resolution temperature measurement was demonstrated with a minimum temperature resolution of 0.01°C and a maximum temperature uncertainty of 0.016°C.

2. Fabrication of phase-shifted fiber Bragg gratings

The experimental setup for writing PSFBGs using femtosecond laser point-by-point technology is shown in Fig. 1. A femtosecond laser (Pharos PH1-10, Light Conversion) with a wavelength of 513 nm, pulse width of 290 fs, single-pulse energy of 30 nJ, and repetition rate of 20 kHz was employed. Femtosecond laser beam is focused onto the core of an unstripped optical fiber, through a mechanical slit and a shutter. A mechanical slit with a width adjustment range from 0 to 5 mm was used for beam shaping to adjust the refractive index modulation area [20]. A Corning SMF-28 fiber was clamped on a high-precision 3D translation stage (Aerotech ABL15010, ANT130LZS, and ANT130V-5), which moved the fiber at a constant speed of 0.1 mm/s to ensure uniform grating periods. The fiber core was observed using an oil-immersion microscope objective (Leica $100 \times$, NA = 1.25), in which both the microscope objective and fiber were immersed in refractive-index-matching oil to minimize distortion caused by the fiber curvature.

The femtosecond laser point-by-point method offers flexibility in adjusting grating parameters such as period, number of periods, resonant wavelength, and reflectivity, making it suitable for fabricating high-quality PSFBGs [21–24]. The grating period was controlled by the shutter frequency and fiber translation speed, while the refractive index modulation in the fiber core was determined by the laser repetition rate, single-pulse energy, and shutter open time. The fabrication process involved three steps:

- (1) Writing 20,000 grating periods with a pitch of $0.534\,\mu m$ in the fiber core, as shown in Fig. 1(b);
- (2) Achieving a π -phase shifted by moving the fiber 0.267 μ m axially with the laser shutter closed (corresponding to 0.5 grating periods);
- (3) Writing another 20,000 grating periods with the shutter open.

During inscription, the transmission spectrum of the PSFBG was monitored using an ASE broadband light source (FiberLake YS1909) and an optical spectrum analyzer (Yokogawa AQ6370C, wavelength resolution: 0.02 nm).

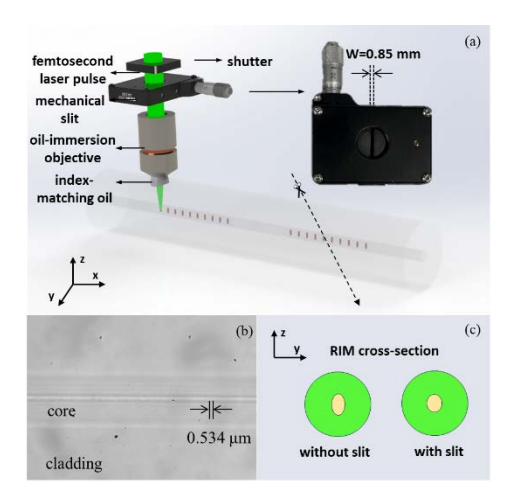


Fig. 1. (a) Experiment setup for PSFBG fabrication by the femtosecond laser point-by-point and slit beam shaping technology, (b) refractive index modulation area induced by a femtosecond laser with slit beam shaping technology, (c) RIM cross-section schematic diagram of two PSFBG samples written without/with slit beam shaping technology, inset: a mechanical silt applied.

A polarization analysis system with higher wavelength resolution (0.1 pm) was used to characterize the PSFBG transmission spectrum and phase-shifted peak bandwidth. This system comprised a tunable laser source (Keysight N7776C), a polarization analyzer (Keysight N7788C), and an optical power meter (Agilent N7744A), enabling measurement of the transmission spectra of two orthogonal linear polarization modes (TE and TM) and PDL. As shown in Fig. 2(a), the initial PSFBG exhibited a distinct phase-shifted peak at 1548.33 nm with a 3 dB bandwidth of 12.0 pm, an insertion loss of 0.25 dB at 1555.00 nm, and a Bragg wavelength separation of 40.3 pm between TE and TM modes, indicating significant birefringence in the grating. The birefringence was calculated as 5.607×10^{-5} using the formula:

$$\Delta n_B = \Delta \lambda / \Lambda \tag{1}$$

where Λ is the grating pitch and $\Delta\lambda$ is the Bragg wavelength difference between TE and TM modes [10,20]. The large birefringence in point-by-point written FBGs arises from the elliptical RIM [25], induced by focused femtosecond laser pulses, in the fiber core cross-section, as shown Fig. 1(c). As described in Refs. [20,25], the birefringence calculation result in the grating with an elliptical or asymmetric RIM via easy formula (1) is highly consistent with the complicated full-vector simulation result. Hence, the formula (1), rather than the full-vector simulation, is employed to calculate the birefringence in the PSFBGs.

The slit beam technology involves modifying the beam prior to reaching the objective lens by introducing a slit. The focused beam waist along each axis depends on the numerical aperture (NA) along that axis, where the NA is determined by the objective focal length (f) and the beam diameter along each axis (D_x, D_y) [25]. The waist radius of the focused beam after passing through the objective lens is:

$$\omega_{oi} = \frac{\lambda}{\pi N A_i} \simeq \frac{\lambda}{\pi} \frac{f}{D_i}, \forall i = \{x, y\}$$
 (2)

To increase the focused beam waist (ω_{oy}) along the Y-axis, the beam diameter (D_y) along the Y-axis has to be reduced. So, the mechanical width-adjustable slit was oriented along the X- axis to change the beam diameter (D_y) , as shown in Fig. 1, and the slit width defines the value of D_y .

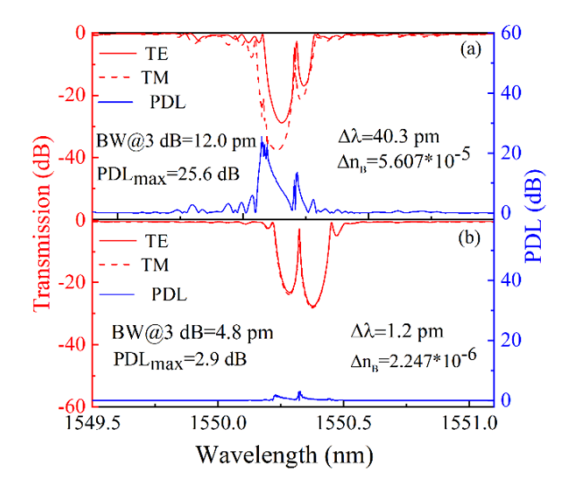


Fig. 2. Transmission spectrum and polarization dependence loss of two PSFBG samples written by the femtosecond laser point-by-point technology (a) without a slit and (b) with a 0.85 mm width slit.

Moreover, to achieve a circular focused spot on the YZ plane after the objective lens, the incident beam diameters, D_x and D_y along the X and Y-axis must meet the following formula [25],

$$\left(1 + \frac{D_x^4}{D_y^4}\right)(1 + \alpha D_y^2) = 4, \quad \alpha = \frac{\ln(2)}{2n^2 f^2}$$
(3)

If the refractive index of n = 1.45 and the focal length of f = 8 mm are adopted, as shown in Fig. 3, the relationship curve between D_x/D_y and D_x is simulated when a circular focused spot is observed on the YZ plane.

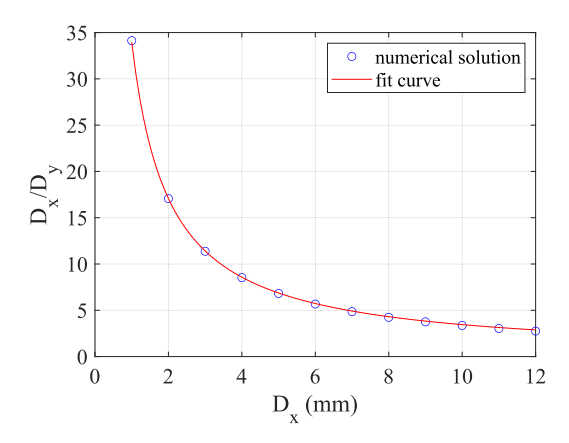


Fig. 3. Numerical simulation of the relationship curve between D_x/D_y and D_x when a circular focused spot is observed on the YZ plane.

Subsequently, we carried out further simulations on the light field distribution of the focused laser spot on the YZ plane under different D_x/D_y ratios of 1, 4, 6.71, and 10 when the incident laser beam diameter of $D_x = 5.70$ mm. It can be observed from Fig. 4 that as the D_x/D_y ratio increases, the focused spot expands along the Y direction, while there is no significant change along the Z direction. Obviously, while the D_x/D_y ratios is 6.71, a circular focused spot is

observed on the YZ plane, as show in Fig. 4(c). In other words, the slit width, i.e. D_y , is required to be adjusted to 0.85 mm in order to achieve a circular focused spot.

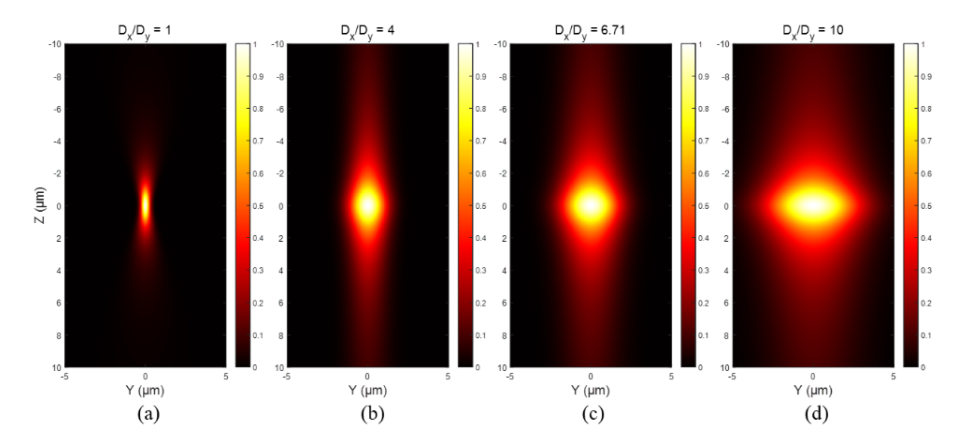


Fig. 4. Numerical simulation of the light field distribution of the focused laser spot on the YZ plane, where $D_x = 5.70$ mm, and the ratio of D_x / D_y is (a) 1, (b) 4, (c) 6.71, and (d) 10, respectively.

The spot radii along the y and z axes after focusing are given by:

$$\omega_{y} = \frac{f\lambda}{\pi W_{y}}, \omega_{z} = \frac{f\lambda}{\pi W_{z}} \tag{4}$$

where W_y and W_z are the beam waists along the y and z axes, f is the objective focal length, and λ is the laser wavelength [1]. So narrower beam waists lead to larger focal spot diameters. In our experiments, using slit beam shaping (Fig. 1(a)), the focal spot size in the y-direction was expanded to make the RIM cross-section nearly circular, reducing birefringence, as shown in Fig. 1(c).

To verify the effectiveness of slit shaping technology in adjusting the refractive index modulation region, the ends of two PSFBG samples were observed via an optical microscope (Leica DM2700M). As shown in Fig. 5(a), the Y and Z dimensions of the RIM cross-section of a PSFBG sample written by the femtosecond laser technology without a slit were measured to be 2.91 and 0.85 μm , respectively. In contrast, as shown in Fig. 5(b), the Y and Z dimensions of the RIM cross-section of another PSFBG sample written by the femtosecond laser technology with a 0.85 mm width slit were measured to be 1.56 and 1.45 μm , respectively. Obviously, the RIM cross-section of the PSFBG sample after shaping was adjusted to an approximate circular spot. As shown in Fig. 2(b), therefore, the Bragg wavelength separation between TE and TM modes was reduced to 1.2 pm after shaping, with a maximum PDL of 2.9 dB and birefringence of 2.247 \times 10⁻⁶ (calculated via (1)). The 3 dB bandwidth of the transmission spectrum narrowed to 4.8 pm, enhancing the wavelength resolution for temperature sensing.

Moreover, to validate the reproducibility of the PS-FBG inscription method above, five PS-FBGs were successfully inscribed under identical fabrication parameters (grating pitch: $0.534 \,\mu\text{m}$, total period number: 40000, π -phase shift: $0.267 \,\mu\text{m}$ at 20000^{th} period, laser wavelength: $513 \, \text{nm}$, pulse width: $290 \, \text{fs}$, single-pulse energy: of $30 \, \text{nJ}$, and repetition rate: $20 \, \text{kHz}$). As summarized in Table 1, all five inscribed grating samples (S1-S5) exhibited nearly identical characteristics, including resonant wavelength (λ_B), reflectivity (R), 3 dB bandwidth (BW), PDL, and birefringence (Δn_B). These results conclusively demonstrate the high repeatability of our slit-beam-shaped femtosecond laser grating fabrication technique.

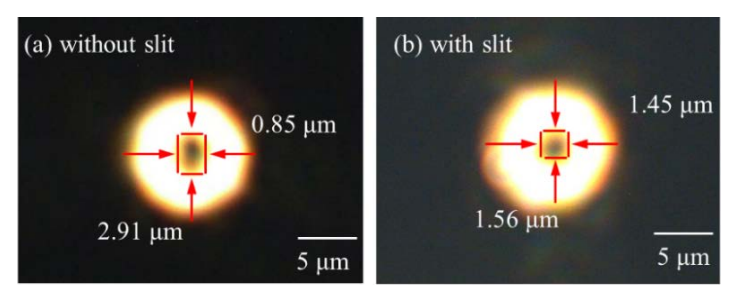


Fig. 5. Cross-section microscope images of two PSFBG samples written by the femtosecond laser point-by-point technology (a) without a slit and (b) with a 0.85 mm width slit.

PSFBG PDL/dB $\Delta n_B / 10^{-6}$ λ_B /nm BW/pm PSFBG₁ 1549.704 4.8 2.9 2.247 PSFBG₂ 1549.716 5.1 3.3 3.135 1549.722 2.925 PSFBG₃ 4.9 3.1 5.0 PSFBG₄ 1549.712 3.2 3.012 1549.698 PSFBG₅ 4.8 3.1 2.544

Table 1. Characteristics of the five PSFBGs inscribed under identical fabrication parameters

3. Temperature characteristics of phase-shifted fiber Bragg gratings

In order to verify that the PSFBG written by use of a femtosecond laser with the slit beam shaping technique can bring higher precision sensing capability, we conducted temperature response characteristic testing experiments on PSFBG. The temperature response of the PSFBG was characterized by use of a polarization analysis system with a wavelength resolution of 0.1 pm. The polarization analysis system consists of a tunable laser (Keysight N7776C), polarization analyzer (Keysight N7788C), optical power meter (Agilent N7744A), as shown in Fig. 6. A thermostatic water bath and a high-precision platinum thermometer (YET-720L) were employed to adjust and measure the grating temperature. The PSFBG was placed inside the water bath, with the high-precision platinum thermometer positioned nearby to monitor the actual temperature at the grating location, compensating for differences between the set temperature and the true temperature.

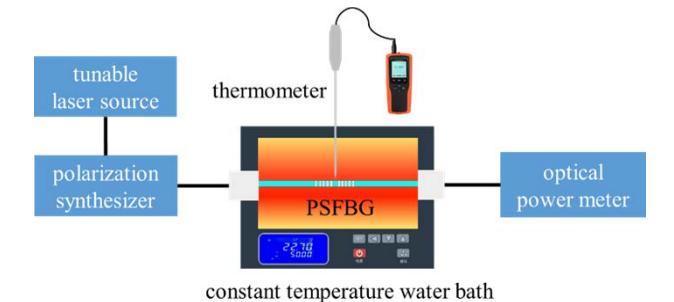


Fig. 6. Experimental setup of high-precision temperature sensing based on the PSFBG.

The water bath temperature was increased from $20\,^{\circ}\text{C}$ to $70\,^{\circ}\text{C}$ in $5\,^{\circ}\text{C}$ increments. At each temperature, the resonant wavelength and transmission spectrum of the PSFBG were measured using the polarization analysis system. To reduce measurement uncertainty, each wavelength

was recorded five times at 1-minute intervals. Figure 7 shows the resonant wavelength shift with temperature, yielding a temperature sensitivity of $10.12 \text{ pm/}^{\circ}\text{C}$ and a determination coefficient $R^2 = 0.999$, indicating a strong linear relationship.

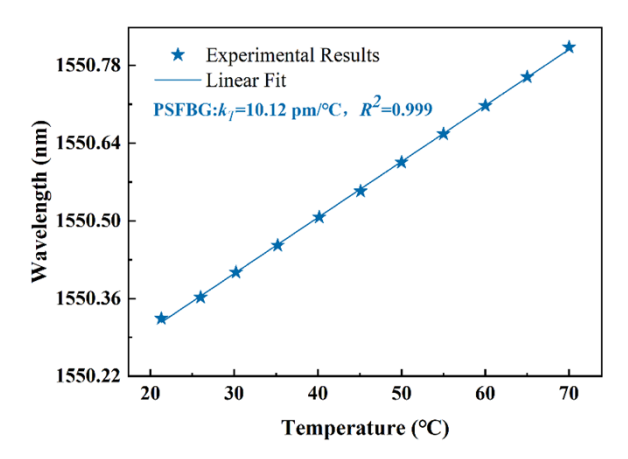


Fig. 7. Temperature response characteristics of PSFBG resonant wavelength.

To evaluate accurately the PSFBG's high-precision sensing capability, the water bath temperature was varied from $55.0~^{\circ}\text{C}$ to $55.5~^{\circ}\text{C}$ in $0.05~^{\circ}\text{C}$ increments. The true temperature was measured using a high-precision platinum thermometer (accuracy: $0.001~^{\circ}\text{C}$). The polarization

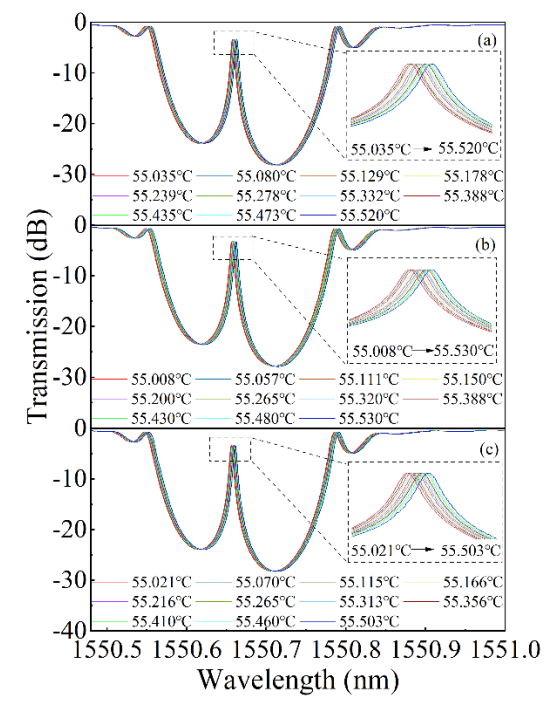


Fig. 8. Transmission spectrum evolution of the PSFBG with the temperature increase from $55.00~^{\circ}\text{C}$ to $55.50~^{\circ}\text{C}$ with a step of $0.05~^{\circ}\text{C}$ while the (a) first, (b) second, and (c) third temperature experiment was done. The insets are the evolution of the phase shifted peak of the PSFBG.

analysis system with high wavelength resolution (0.1 pm) was used to characterize the transmission spectrum of the PSFBG. At each temperature, the transmission spectrum and resonant wavelength of the PSFBG were recorded five times at 1-minute intervals to reduce measurement uncertainty. Three repeated tests were conducted to assess repeatability and reliability of the PSFBG temperature response characteristics.

Figure 8 shows the transmission spectra during the three tests, with the inset indicating a consistent redshift of the phase-shifted peak with increasing temperature. Figure 9 plots the resonant wavelength versus temperature for each test, yielding sensitivities of 10.53, 10.88, and $10.72 \text{ pm/}^{\circ}\text{C}$, with $R^2 = 0.9991$, 0.9993, and 0.9997, respectively. Thus, the average temperature

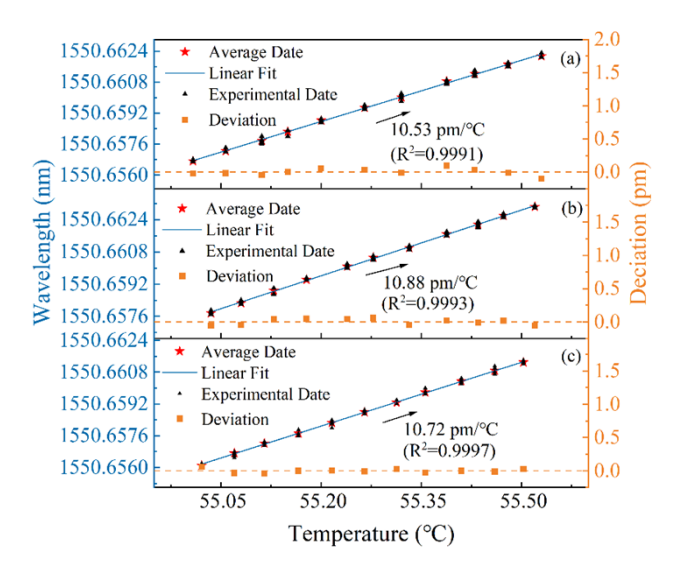


Fig. 9. Resonant wavelength of the PSFBG with the temperature increase from $55.00\,^{\circ}$ C to $55.50\,^{\circ}$ C with a step of $0.05\,^{\circ}$ C while the (a) first, (b) second, and (c) third temperature experiment was done.

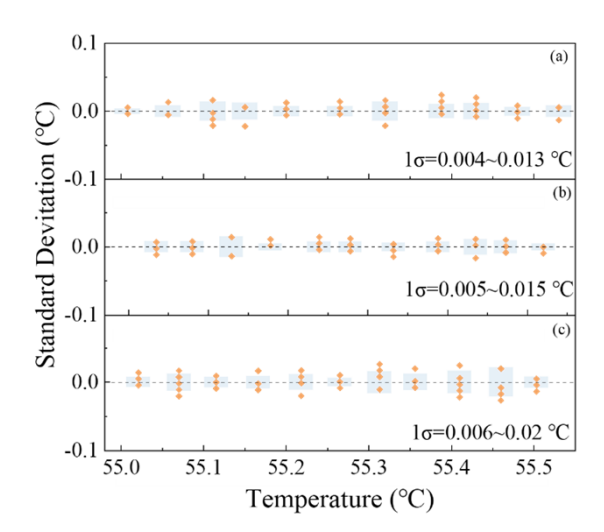


Fig. 10. Measured temperature standard deviation of the PSFBG at each temperature from $55.00 \,^{\circ}\text{C}$ to $55.50 \,^{\circ}\text{C}$ with a step of $0.05 \,^{\circ}\text{C}$ while the (a) first, (b) second, and (c) third temperature experiment was done.

sensitivity of the PSFBG was 10.71 pm/°C. The measured temperature values and their standard deviations are shown in Fig. 10, with standard deviation ranges of 0.004–0.013 °C, 0.005–0.015 °C, and 0.006–0.020 °C for the three tests. Thus, the average standard deviation range was 0.005–0.016 °C, leading to a maximum temperature uncertainty of 0.016 °C. Moreover, the phase-shifted peak of the PSFBG was measured by the polarization analysis system with a high wavelength resolution of 0.1 pm. The temperature resolution of the PSFBG sensor is calculated by use of the wavelength resolution (0.1 pm) of the polarization analysis system and the temperature sensitivity (10.71 pm/°C) of the PSFBG, e.g. 0.1 pm \div 10.71 pm/°C = 0.0093 °C \approx 0.01 °C. Thus, the temperature resolution of our proposed PSFBG sensor was achieved to be 0.01 °C, which reflects the minimum distinguishable temperature change of the grating sensor.

The measurement accuracy of optical fiber grating temperature sensors mainly depends on the wavelength resolution of the grating and the anti-interference ability of the resonant wavelength. We utilized the femtosecond laser slit beam shaping technology to reduce the 3 dB bandwidth of the phase-shifted peak of the PSFBG from 12.0 pm to 4.8 pm, thereby improving the wavelength resolution by an order of magnitude. Moreover, the birefringence of the PSFBG was reduced from 5.607×10^{-5} to 2.247×10^{-6} , which significantly enhanced the anti-interference ability (i.e., wavelength stability) of the resonant wavelength during the temperature measurement process. As a result, the maximum uncertainty of the PSFBG temperature measurement was reduced to 0.016 °C. It can be seen that the developed PSFBG temperature sensor has excellent temperature resolution and measurement accuracy.

4. Conclusion

We demonstrated the inscription of a high-quality π -phase-shifted fiber Bragg grating using femtosecond laser point-by-point technology with slit beam shaping, reducing PDL from 25.6 dB to 2.9 dB and narrowing the 3 dB bandwidth of the phase-shifted peak from 12.0 pm to 4.8 pm, thereby enhancing wavelength resolution. The temperature response of the PSFBG was characterized using a polarization analysis system and thermostatic water bath, achieving a sensitivity of 10.71 pm/°C and demonstrating high-precision measurement with a minimum resolution of 0.01°C and maximum uncertainty of 0.016°C. This is primarily attributed to the reduction of the PSFBG's birefringence from 5.607×10^{-5} to 2.247×10^{-6} using the slit beam shaping technique, which greatly enhances the stability of the resonant wavelength of the phase-shifted peak and the measurement accuracy of the grating temperature sensor. Moreover, the femtosecond-laser-inscribed grating sensor can withstand a high temperature and have excellent long-term thermal stability and repeatability [26]. Therefore, these results highlight the PSFBG's potential for high-resolution and high-precision temperature sensing in applications such as semiconductor manufacturing, biomedicine, and oil well exploration.

Funding. National Key Research and Development Program of China (2023YFB3209500); National Natural Science Foundation of China (6222510, 62374111, U22A2088, T2421003); Shenzhen Science and Technology Innovation Program (JCYJ20220818095800001, ZDSYS20220606100405013).

Disclosures. The authors declare no conflicts of interest.

Data availability. Data underlying the results presented in this paper are not publicly available at this time but may be obtained from the authors upon reasonable request.

References

- J. He, R. X. Chen, X. Z. Xu, et al., "Slit beam shaping for femtosecond laser point-by-point inscription of highly localized fiber Bragg grating," J. Lightwave Technol. 40(16), 5722–5728 (2022).
- Z. L. Rani, X. He, Y. J. Rao, et al., "Fiber-optic microstructure sensors: a review," Photonic Sens. 11(2), 227–261 (2021).
- 3. B. N. Liu, J. X. Luo, S. Liu, *et al.*, "A probe-shaped sensor with FBG and fiber-tip bubble for pressure and temperature sensing," Photonic Sens. **11**(4), 411–417 (2021).
- J. He, B. J. Xu, X. Z. Xu, et al., "Review of femtosecond-laser-inscribed fiber Bragg gratings: fabrication technologies and sensing applications," Photonic Sens. 11(2), 203–226 (2021).

- D. Srivastava, B. Das, U. Tiwari, et al., "Experimental and theoretical investigation of phase shifted fiber Bragg grating for temperature measurement," *IEEE International Conference on Power, Control, Signals and Instrumentation Engineering (ICPCSI)*, 754–757 (2017).
- A. S. Chernikov, K. S. Khorkov, D. A. Kochuev, et al., "Line-by-line fiber Bragg grating fabrication by femtosecond laser radiation," Vii International Conference Modern Nanotechnologies and Nanophotonics for Science and Industry (2019).
- X. Xu, J. He, C. Liao, et al., "Sapphire fiber Bragg gratings inscribed with a femtosecond laser line-by-line scanning technique," Opt. Lett. 43(19), 4562–4565 (2018).
- P. Lu, S. J. Mihailov, H. Ding, et al., "Plane-by-plane inscription of grating structures in optical fibers," J. Lightwave Technol. 36(4), 926–931 (2018).
- K. Chah, D. Kinet, M. Wuilpart, et al., "Femtosecond-laser-induced highly birefringent Bragg gratings in standard optical fiber," Opt. Lett. 38(4), 594–596 (2013).
- N. Jovanovic, J. Thomas, R. J. Williams, et al., "Polarization-dependent effects in point-by-point fiber Bragg gratings enable simple, linearly polarized fiber lasers," Opt. Express 17(8), 6082–6095 (2009).
- Y. Lai, K. Zhou, K. Sugden, et al., "Point-by-point inscription of first-order fiber Bragg grating for C-band applications," Opt. Express 15(26), 18318–18325 (2007).
- H. Xu, X. Zheng, W. Zhao, et al., "High precision, small size and flexible fbg strain sensor for slope model monitoring," Sensors 19(12), 2716 (2019).
- J. G. Chen, Q. W. Liu, and Z. Y. He, "High-resolution simultaneous measurement of strain and temperature using π-phase-shifted FBG in polarization maintaining fiber," J. Lightwave Technol. 35(22), 4838–4844 (2017).
- A. I. Azmi, D. Sen, W. Sheng, et al., "Performance enhancement of vibration sensing employing multiple phase-shifted fiber Bragg grating," J. Lightwave Technol. 29(22), 3453–3460 (2011).
- Z. Sun, Y. Lv, M. Zou, et al., "High precision temperature sensor based on π-phase-shifted FBG and OFDR system," Conference on Lasers and Electro-Optics (CLEO), (2024).
- R. Pashaie and M. Vahedi, "Simultaneous measurement of temperature and strain of a fixed composite cantilever using a π-PSFBG sensor," Opt. Quant. Electron. 54(2), 85 (2022).
- 17. H. Cheng, L. Wang, R. R. Xiao, *et al.*, "Temperature sensing of π-PSFBG with ITO film coated by PLD method," Optik **262**, 169289 (2022).
- F. Zhang, X. Yan, X. N. Zhang, et al., "Simulation of wide wavelength tuning of As2Se3 π-PSFBG narrow band fiber laser based on temperature and strain," Laser Phys. Lett. 18(4), 045101 (2021).
- Z. Q. Sun, X. P. Xiao, W. L. Zhao, et al., "High-precision distributed temperature sensor based on phase-shifted FBGs interrogated by OFDR," J. Lightwave Technol. 43(5), 2357–2362 (2025).
- X. Z. Xu, J. He, J. He, et al., "Slit beam shaping for femtosecond laser point-by-point inscription of high-quality fiber Bragg gratings," J. Lightwave Technol. 39(15), 5142–5148 (2021).
- Y. Lv, Y. Wei, S. T. Zhu, et al., "Femtosecond laser-induced refractive index modulation of 2D perovskites for phase-modulated holographic neural networks," ACS Photonics 12(7), 3618–3625 (2025).
- P. Zeil, C. Voigtländer, J. Thomas, et al., "Femtosecond laser-induced apodized Bragg grating waveguides," Opt. Lett. 38(13), 2354–2356 (2013).
- 23. S. Suntsov, D. Abdollahpour, D. G. Papazoglou, *et al.*, "Femtosecond laser induced plasma diffraction gratings in air as photonic devices for high intensity laser applications," Appl. Phys. Lett. **94**(25), 251104 (2009).
- H. C. Guo, H. B. Jiang, Y. Fang, et al., "The pulse duration dependence of femtosecond laser induced refractive index modulation in fused silica," J. Opt. A: Pure Appl. Opt. 6(8), 787–790 (2004).
- P. Roldán-Varona, D. Pallarés-Aldeiturriaga, L. Rodríguez-Cobo, et al., "Slit beam shaping technique for femtosecond laser inscription of enhanced plane-by-plane FBGs," J. Lightwave Technol. 38(16), 4526–4532 (2020).
- B. J. Xu, J. He, B. Du, et al., "Femtosecond laser point-by-point inscription of an ultra-weak fiber Bragg grating array for distributed high-temperature sensing," Opt. Express 29(20), 32615–32626 (2021).